Geophysical Journal International

Geophys. J. Int. (2018) **214,** 1088–1104
Advance Access publication 2018 April 30
GJI Seismology

doi: 10.1093/gji/ggy173

Determination of rock-sample anisotropy from *P*- and *S*-wave traveltime inversion

Ivan Pšenčík,[1] Bohuslav Růžek,[1] Tomáš Lokajíček[2] and Tomáš Svitek[2]

[1]*Institute of Geophysics, The Czech Academy of Sciences, Boční II,* 141 31 *Prague* 4*, Czech Republic E-mail: ip@ig.cas.cz*
[2]*Institute of Geology, The Czech Academy of Sciences, Rozvojová* 269, 165 00 *Prague* 6*, Czech Republic*

Accepted 2018 April 27. Received 2018 February 24; in original form 2017 November 3

SUMMARY

We determine anisotropy of a rock sample from laboratory measurements of *P*- and *S*-wave traveltimes using weak-anisotropy approximation and parametrization of the medium by a special set of anisotropy parameters. For the traveltime inversion, we use first-order velocity expressions in the weak-anisotropy approximation, which allow to deal with *P* and *S* waves separately. Each wave is described by 15 anisotropy parameters, 9 of which are common for both waves. The parameters allow an approximate construction of separate *P*- or common *S*-wave phase-velocity surfaces. Common *S*-wave concept is used to simplify the treatment of *S* waves. In order to obtain all 21 anisotropy parameters, *P*- and *S*-wave traveltimes must be inverted jointly. The proposed inversion scheme has several advantages. As a consequence of the use of weak-anisotropy approximation and assumed homogeneity of the rock sample, equations used for the inversion are linear. Thus, the inversion procedure is non-iterative. In the approximation used, phase and ray velocities are equal in their magnitude and direction. Thus, analysis whether the measured velocity is the ray or phase velocity is unnecessary. Another advantage of the proposed inversion scheme is that, thanks to the use of the common *S*-wave concept, it does not require identification of *S*-wave modes. It is sufficient to know the two *S*-wave traveltimes without specification, to which *S*-wave mode they belong. The inversion procedure is tested first on synthetic traveltimes and then used for the inversion of traveltimes measured in laboratory. In both cases, we perform first the inversion of *P*-wave traveltimes alone and then joint inversion of *P*- and *S*-wave traveltimes, and compare the results.

Key words: Body waves; Seismic anisotropy; Seismic tomography.

INTRODUCTION

There were many attempts in the past to estimate anisotropy of rock samples from rock-physics laboratory measurements. Among them, see, for example Jech (1991), Arts *et al.* (1991), Arts (1993), Vestrum (1994), Mahmoudian *et al.* (2014), Svitek *et al.* (2014) or Lokajíček & Svitek (2015). Great advantage of these experiments is that laboratory measurements can provide a sounding of a sample from all directions, and thus give a chance to recover the complete stiffness tensor. This, however, requires to record not only *P* wave, but also both *S* waves. In our study, we use *P*- and *S*-wave traveltimes obtained either numerically from two-point ray tracing (Gajewski & Pšenčík 1990) or from laboratory measurements using the technique developed by Svitek *et al.* (2014) and Lokajíček & Svitek (2015). The use of *S* waves brings an additional and independent information useful in the inversion, but it also introduces problems. *S* waves usually arrive in the *P*-wave coda, and thus their detection is less accurate. There are generally two *S* waves propagating in anisotropic media. In some directions, they arrive separately, in other directions they arrive coupled, indistinguishable. Moreover, in different directions, they may arrive in a different order. This requires their identification, most naturally by their polarization, which, however, is not a very accurate and reliable process. Another problem connected with the *S*-wave propagation in anisotropic media is the possibility of their multiple arrivals. As Grechka (2017) shows, there might be up to 18 *S*-wave arrivals along a straight line from a source to a receiver in a homogeneous anisotropic medium. All the above-mentioned problems must be considered when dealing with *S* waves.

In this paper, we wish to contribute to the ongoing research by presenting an inversion scheme based on (1) a special parametrization of a medium, (2) use of the weak-anisotropy approximation and (3) a special treatment of *S* waves. All three mentioned items should simplify the inversion and make it more reliable.

(1) The special parametrization consists in the use of a special set of parameters, which we call anisotropy parameters. Anisotropy parameters characterize deviations of the studied anisotropic medium from a reference isotropic medium. They represent a generalization of Thomsen's parameters (Thomsen 1986) to anisotropic media of arbitrary symmetry, strength and orientation. They are an alternative to either elastic moduli in the Voigt notation or elements of stiffness tensor, or to their density-normalized counterparts. Anisotropy parameters take into account natural combinations of some of the moduli (see, e.g. Thomsen's δ parameter), which are usually difficult to resolve separately. This makes them a practical choice for the inversion.

(2) In the weak-anisotropy approximation, which we are using in our inversion scheme, we can expand the formulae for various attributes of seismic waves (phase or ray velocities, polarization, etc.) in terms of anisotropy parameters, and most often keep just the first-order terms of the expansion, which are linear with respect to the anisotropy parameters. This leads to simplified formulae, which, as many studies show, are, however, still sufficiently accurate even in moderately anisotropic media. Among many advantages, the first-order formulae in the weak-anisotropy approximation allow to separate the expressions for *P*-wave phase or ray velocities from those for *S* waves. Such a separation leads to the reduction of the number of anisotropy parameters specifying *P*- or *S*-wave propagation; in general (triclinic) anisotropy, it is from 21 to 15. In this general case, nine parameters are common for *P* and *S* waves, six appear only in the formulae describing *P*-wave attributes and remaining six appear only in the formulae describing *S*-wave attributes. In this study, we use the first-order approximation of exact expressions for the square of the *P*- and common *S*-wave velocities. In the used approximation, ray and phase velocities are considered equal, both in their size and direction, and are linear with respect to anisotropy parameters. This might seem a rough approximation, but as Růžek & Pšenčík (2016) show, presence of noise of a realistic size in data outweighs effects of inaccurate velocity approximation. In the following, we, therefore, use just the term velocity, and do not distinguish between ray and phase velocities. Useful consequence of the equality of ray and phase velocities is no need for analysis whether phase or ray velocity is measured (Dellinger & Vernik 1994).

(3) Our special treatment of *S* waves consists in treating the two separate *S* waves as a single common *S* wave, which propagates with the ray velocity, whose square is an average of squares of ray velocities of separate *S* waves, $v_S^2 = \frac{1}{2}(v_{S1}^2 + v_{S2}^2)$, where v_{S1} and v_{S2} are the ray velocities of S1 and S2 waves, respectively. Common *S* wave concept plays an important role in the computation of coupled *S* waves. For details, see, for example, Farra & Pšenčík (2008) or Pšenčík *et al.* (2012). The advantage of this formulation is the simplicity of the expression for the square of the velocity of the common *S* wave. It contains no square roots appearing in formulae for separate waves, and provides, as in case of *P* waves, a linear relation between the square of the velocity and anisotropy parameters. Useful consequence of the use of the common *S* wave is no need for the identification of polarization of recorded *S*-wave modes, which may arrive to different receivers in a different order.

Since we consider the rock sample to be homogeneous, the above-described specifications result in simple explicit algebraic equations relating linearly squared *P*- and common *S*-wave velocities with the sought anisotropy parameters. Thus, there is no need for iterative solution of the equations.

Preliminary tests of the proposed inversion procedure can be found in Pšenčík *et al.* (2017).

The paper has the following structure. In the following section, anisotropy parameters are introduced and their usefulness for our study is discussed. Then the first-order approximations of squares of *P*- and common *S*-wave velocities expressed in terms of anisotropy parameters are given and briefly discussed. In the following section, it is shown how the expressions for *P*- and common *S*-wave velocities are used in the formation of the system of equations to be inverted. This section is followed by the section, in which we describe procedures used for obtaining synthetic and laboratory data. In the section after it, we present results of the inversion tests and their discussion. General discussion of obtained results and encountered problems can be found in the concluding section. The main text is supplemented by three Appendices. Appendix A contains description of the construction of model covariance matrices and of the way in which errors of model parameters are estimated. In Appendix B, maximum likelihood solution used to solve the system of linear equations is briefly described. The last Appendix C contains the matrix of density-normalized elastic moduli used in the synthetic experiment.

THEORETICAL BACKGROUND

Anisotropy parameters

For the parametrization of the medium, we use 21 parameters, which may be used to specify an anisotropic medium of arbitrary symmetry, strength or orientation. The parameters are related to the density-normalized elastic moduli in the Voigt notation, $A_{\alpha\beta}$, in the following way:

$$\epsilon_x = \frac{A_{11} - \alpha^2}{2\alpha^2}, \quad \epsilon_y = \frac{A_{22} - \alpha^2}{2\alpha^2}, \quad \epsilon_z = \frac{A_{33} - \alpha^2}{2\alpha^2},$$

$$\chi_x = \frac{A_{14} + 2A_{56}}{\alpha^2}, \quad \chi_y = \frac{A_{25} + 2A_{46}}{\alpha^2}, \quad \chi_z = \frac{A_{36} + 2A_{45}}{\alpha^2},$$

$$\eta_x = \frac{2(A_{23} + 2A_{44}) - A_{22} - A_{33}}{2\alpha^2}, \quad \eta_y = \frac{2(A_{13} + 2A_{55}) - A_{33} - A_{11}}{2\alpha^2},$$

$$\eta_z = \frac{2(A_{12} + 2A_{66}) - A_{11} - A_{22}}{2\alpha^2},$$

$$\xi_{24} = \frac{A_{14} + 2A_{56} - A_{24}}{\alpha^2}, \quad \xi_{34} = \frac{A_{14} + 2A_{56} - A_{34}}{\alpha^2}, \quad \xi_{15} = \frac{A_{25} + 2A_{46} - A_{15}}{\alpha^2},$$

$$\xi_{35} = \frac{A_{25} + 2A_{46} - A_{35}}{\alpha^2}, \quad \xi_{16} = \frac{A_{36} + 2A_{45} - A_{16}}{\alpha^2}, \quad \xi_{26} = \frac{A_{36} + 2A_{45} - A_{26}}{\alpha^2},$$

$$\gamma_x = \frac{A_{44} - \beta^2}{2\beta^2}, \quad \gamma_y = \frac{A_{55} - \beta^2}{2\beta^2}, \quad \gamma_z = \frac{A_{66} - \beta^2}{2\beta^2},$$

$$\epsilon_{45} = \frac{A_{45}}{\beta^2}, \quad \epsilon_{46} = \frac{A_{46}}{\beta^2}, \quad \epsilon_{56} = \frac{A_{56}}{\beta^2}. \tag{1}$$

We call the above parameters *anisotropy parameters*. The symbols α and β in eq. (1) denote *P*- and *S*-wave velocities of a reference isotropic medium. They can be chosen as arbitrary non-zero quantities, for example, as $\alpha^2 = A_{33}$ and $\beta^2 = A_{55}$, which was Thomsen's (1986) choice. In this paper, we choose them close to the mean of *P*- and *S*-wave velocities derived from traveltime data.

Anisotropic parameters (1) represent a generalization of Thomsen's (1986) parameters introduced for transversely isotropic media with vertical axis of symmetry (VTI media). They have a close relation to the so-called weak-anisotropy parameters, see Farra *et al.* (2016), which are slightly modified parameters introduced by Mensch & Rasolofosaon (1997), see also Pšenčík & Gajewski (1998) and Farra & Pšenčík (2003).

Since properties of anisotropy parameters are similar to properties of weak-anisotropy parameters, we refer to their detailed description by Farra *et al.* (2016). Here, we mention only their most important properties.

All anisotropy parameters are related *linearly* to the density-normalized elastic moduli $A_{\alpha\beta}$ or to the density-normalized elements of the stiffness tensor a_{ijkl}. Important consequence of this linear relation is possibility to transform anisotropy parameters from one coordinate system to another. This is impossible with, for example, Thomsen's parameters .

The possibility to choose the *P*- and *S*-wave reference velocities α and β is especially useful in linearized inversions, when magnitudes of anisotropic updates are required to be small for the inversion to be accurate. The magnitudes of anisotropy parameters can be optimized for a given inversion. It is, however, important to emphasize that the parametrization by anisotropy parameters is not limited to linear inversions or to weak anisotropy.

The useful advantage of anisotropy parameters is that they are all dimensionless and can be designed to have comparable sizes. Comparability of the size of anisotropy parameters is a useful property, especially in the inversion.

Another important advantage of anisotropy parameters, which we employ in the following, is that in combination with the use of weak anisotropy approximation they lead to completely separate expressions for *P* and S waves. This in turn leads to the reduction of the number of anisotropy parameters specifying *P*- and *S*-wave propagation.

Relations between velocities and anisotropy parameters

The relation between observed traveltimes and sought anisotropy parameters is controlled by *P*- and *S*-wave velocities. Exact expressions for ray or phase velocities are quite complex. Instead of them, we are using approximate expressions, specifically first-order weak-anisotropy approximations of the squares of *P*- and common *S*-wave velocities, respectively. We denote them by $\widetilde{v}_P^2$ and $\widetilde{v}_S^2$, respectively. We use expressions derived under the assumptions of no differences between the directions **n** and **N** of phase and ray velocities, respectively, and equality of squares of both velocities. Their derivation and tests of their accuracy can be found in papers referred below. Here, we use them expressed in terms of anisotropy parameters.

The square of the first-order *P*-wave velocity formula for anisotropy of arbitrary symmetry in the weak-anisotropy approximation follows from eq. (17a) of Pšenčík & Gajewski (1998) or eq. (A4) of Farra & Pšenčík (2003):

$$\begin{aligned}\widetilde{v}_P^2(\epsilon_i, N_j) = \alpha^2\Big(&1 + 2(\epsilon_x N_1^2 + \epsilon_y N_2^2 + \epsilon_z N_3^2 + \eta_x N_2^2 N_3^2 + \eta_y N_1^2 N_3^2 + \eta_z N_1^2 N_2^2)\\ &+4N_2N_3(\chi_x - \xi_{24}N_2^2 - \xi_{34}N_3^2) + 4N_3N_1(\chi_y - \xi_{35}N_3^2 - \xi_{15}N_1^2)\\ &+4N_1N_2(\chi_z - \xi_{16}N_1^2 - \xi_{26}N_2^2)\Big).\end{aligned} \tag{2}$$

For tests of accuracy of eq. (2), see Farra & Pšenčík (2016).

The square of the first-order common *S*-wave velocity formula for anisotropy of arbitrary symmetry in the weak-anisotropy approximation follows from eq. (19) of Farra & Pšenčík (2008):

$$\begin{aligned}\widetilde{v}_S^2(\epsilon_i, N_j) = \beta^2\Big(&1 + \gamma_x(N_2^2 + N_3^2) + \gamma_y(N_1^2 + N_3^2) + \gamma_z(N_1^2 + N_2^2)\\ &+\epsilon_{45}N_1N_2 + \epsilon_{46}N_1N_3 + \epsilon_{56}N_2N_3\Big) - \alpha^2\Big(\eta_x N_2^2N_3^2 + \eta_y N_3^2N_1^2 + \eta_z N_1^2N_2^2\\ &+\xi_{24}N_2N_3(1 - 2N_2^2) + \xi_{34}N_2N_3(1 - 2N_3^2) + \xi_{15}N_3N_1(1 - 2N_1^2)\\ &+\xi_{35}N_3N_1(1 - 2N_3^2) + \xi_{16}N_1N_2(1 - 2N_1^2) + \xi_{26}N_1N_2(1 - 2N_2^2)\Big).\end{aligned} \tag{3}$$

We can see that besides anisotropy parameters and components of the ray vector **N**, eqs (2) and (3) also contain the reference *P*- and *S*-wave velocities α and β. It is important to emphasize that their appearance is related to the use of anisotropy parameters. Eqs (2) and (3) are *independent* of α and β. Also note that in VTI media, formula (2) reduces to the square of eq. (16a) and formula (3) to the average of squares of eqs (16b) and (16c) of Thomsen (1986). For zero-valued anisotropy parameters, eqs (2) and (3) yield squares of *P*- and *S*-wave velocities α and β of the reference isotropic medium.

A detailed inspection of eqs (2) and (3) implies that anisotropy parameters ϵ_x, ϵ_y, ϵ_z, χ_x, χ_y and χ_z appear only in eq. (2) for *P*-waves. Parameters γ_x, γ_y, γ_z, ϵ_{45}, ϵ_{46} and ϵ_{56} appear only in eq. (3) for common *S* wave. The remaining nine anisotropy parameters η_x, η_x, η_x, ξ_{24}, ξ_{34}, ξ_{15}, ξ_{35}, ξ_{16} and ξ_{26} are common for both waves, they appear in both eqs (2) and (3). Each of the eqs (2) and (3) depends on only 15 anisotropy parameters.

It is of interest to note that while parameters ϵ and γ in eq. (1) have a clear relation to Thomsen's (1986) parameters of the same notation, our parameters η have relation to anellipticity parameters η and parameters σ used in exploration seismics. In case of *P* waves, η parameters used in eq. (2) relate to anellipticity parameters η, see Alkhalifah & Tsvankin (1995) or Tsvankin & Grechka (2011), see eqs (1.88)–(1.90). In case of *S* waves, η parameters used in eq. (3) relate to parameters σ, see, Tsvankin & Grechka (2011), eq. (6.13).

In the following tests, we specify the ray vector **N** by the azimuth ϕ and polar angle θ

$$\mathbf{N} \equiv (\cos\varphi\cos\theta, \sin\varphi\cos\theta, \sin\theta). \tag{4}$$

SYSTEM OF LINEAR EQUATIONS AND ITS SOLUTION

For N^P measurements of *P*-wave traveltimes t_i^P, $i = 1, 2, .., N^P$, and N^S measurements of common *S*-wave traveltimes t_j^S, $j = 1, 2, .., N^S$, eqs (2) and (3) yield a system of $N^P + N^S$ linear equations for the determination of anisotropy parameters. Common *S*-wave traveltimes t_j^S are determined from the relation:

$$\left(t_j^S\right)^2 = 2\left(t_j^{S1}\right)^2\left(t_j^{S2}\right)^2 / \left[\left(t_j^{S1}\right)^2 + \left(t_j^{S2}\right)^2\right], \tag{5}$$

which corresponds to the average of squared S1- and S2-wave velocities. Here, t_j^{S1} and t_j^{S2} are synthetic or observed traveltimes of faster S1 and slower S2 wave, respectively. If only *P*-wave traveltimes are used, one can determine 15 anisotropy parameters, if only *S*-wave traveltimes are used, one can determine different 15 anisotropy parameters. If traveltimes of both waves are used, all 21 anisotropy parameters can be determined. The resulting system of eqs (2) and (3) can be rewritten to the matrix form:

$$\mathbf{Gm} = \mathbf{d}. \tag{6}$$

In eq. (6), **G** represents the $(N^P + N^S) \times M$ forward operator matrix. $N^P + N^S$ is the number of observations and M is the number of sought anisotropy parameters, generally $M = 21$. The rows of matrix **G** resulting from *P*-wave traveltime measurements (eq. 2) have the form

$$\begin{aligned}&(N_1^2 \quad N_2^2 \quad N_3^2 \quad 2N_2N_3 \quad 2N_3N_1 \quad 2N_1N_2 \quad N_2^2N_3^2 \quad N_3^2N_1^2 \quad N_1^2N_2^2 \quad -2N_2^3N_3\\ &-2N_3^3N_2 \quad -2N_1^3N_3 \quad -2N_3^3N_1 \quad -2N_1^3N_2 \quad -2N_2^3N_1 \quad 0 \quad 0 \quad 0 \quad 0 \quad 0 \quad 0).\end{aligned} \tag{7}$$

The rows resulting from *S*-wave traveltime measurements (eq. 3) have the form

$$\begin{aligned}&(0 \quad 0 \quad 0 \quad 0 \quad 0 \quad 0 \quad -N_2^2N_3^2 \quad -N_3^2N_1^2 \quad -N_1^2N_2^2\\ &-N_2N_3(1-2N_2^2) \quad -N_2N_3(1-2N_3^2) \quad -N_1N_3(1-2N_1^2)\\ &-N_1N_3(1-2N_3^2) \quad -N_1N_2(1-2N_1^2) \quad -N_1N_2(1-2N_2^2)\\ &r^2(1-N_1^2) \quad r^2(1-N_2^2) \quad r^2(1-N_3^2) \quad r^2N_1N_2 \quad r^2N_1N_3 \quad r^2N_2N_3 \quad .\end{aligned} \tag{8}$$

Here, N_i are components of the unit ray vector **N** and r is the ratio of the *S*- and *P*-wave reference velocities α and β, $r = \beta/\alpha$.

The symbol **m** in eq. (6) denotes the vector of model parameters to be determined. It generally consists of 21 anisotropy parameters (1) and has the form

$$\mathbf{m} \equiv (\epsilon_x, \epsilon_y, \epsilon_z, \chi_x, \chi_y, \chi_z, \eta_x, \eta_y, \eta_z, \xi_{24}, \xi_{34}, \xi_{15}, \xi_{35}, \xi_{16}, \xi_{26}, \gamma_x, \gamma_y, \gamma_z, \epsilon_{45}, \epsilon_{46}, \epsilon_{56})^T. \tag{9}$$

The symbol T indicates transposition.

The vector **d** in (6) is the data vector, and for *P* wave, it has the form

$$\mathbf{d}_P \equiv \frac{1}{2}\left(\left(\frac{s_1}{\alpha t_1^P}\right)^2 - 1, \left(\frac{s_2}{\alpha t_2^P}\right)^2 - 1, \ldots., \left(\frac{s_N}{\alpha t_{N^P}^P}\right)^2 - 1\right)^T. \tag{10}$$

For common *S* wave, it reads:

$$\mathbf{d}_S \equiv \left(\left(\frac{s_1}{\alpha t_1^S}\right)^2 - r^2, \left(\frac{s_2}{\alpha t_2^S}\right)^2 - r^2, \ldots., \left(\frac{s_N}{\alpha t_{N^S}^S}\right)^2 - r^2\right)^T. \tag{11}$$

In eqs (10) and (11), s_i are the source–receiver distances. In the experiments considered in this paper, they are all equal to the diameter of the spherical rock sample.

Simple and straightforward solution of the system of eqs (6) can be obtained, for example, by using the pseudoinverse matrix $\mathbf{G}^\dagger$ of $\mathbf{G}$, see Appendix A:

$$\mathbf{m} = \mathbf{G}^\dagger \mathbf{d}. \tag{12}$$

In case of inhomogeneous distribution of errors, the maximum likelihood approach is more appropriate for getting results. Using such an approach, all involved equations should be weighted according to the uncertainty of data vector $\mathbf{d}$. Since we expect generally larger traveltime errors of S wave than of P wave, we propose different weighting of P- and S-wave equations as described in more details in Appendices A and B. Thus, the inversion is given as

$$\mathbf{m} = (\mathbf{QG})^\dagger(\mathbf{Qd}), \tag{13}$$

where the weighting matrix $\mathbf{Q}$ is defined in eq. (B2).

DATA USED FOR THE INVERSION

Two data sets are used in the following inversion experiments, synthetic and laboratory traveltimes. The same configuration is used in tests with both data sets. Spherical rock samples used for synthetic as well as laboratory experiments are sounded in 132 different directions by P and S waves. Traveltimes are measured between couples of diametrically situated sources and receivers of P and S waves, distributed regularly on the spherical sample with steps in angles ϕ and θ, see eq. (4), equal 15°. The coverage of the spherical sample is shown in Fig. 1. For a more detailed description of the measurement set-up, see Svitek *et al.* (2014) or Lokajíček & Svitek (2015). Strength of the studied anisotropy is determined from the expression $2(c_{\max} - c_{\min})/(c_{\max} + c_{\min}) \times 100$ per cent. Here, $c_{\min}$ and $c_{\max}$ represent minimum and maximum phase velocities, respectively, found from measurements made in a dense system of randomly distributed directions.

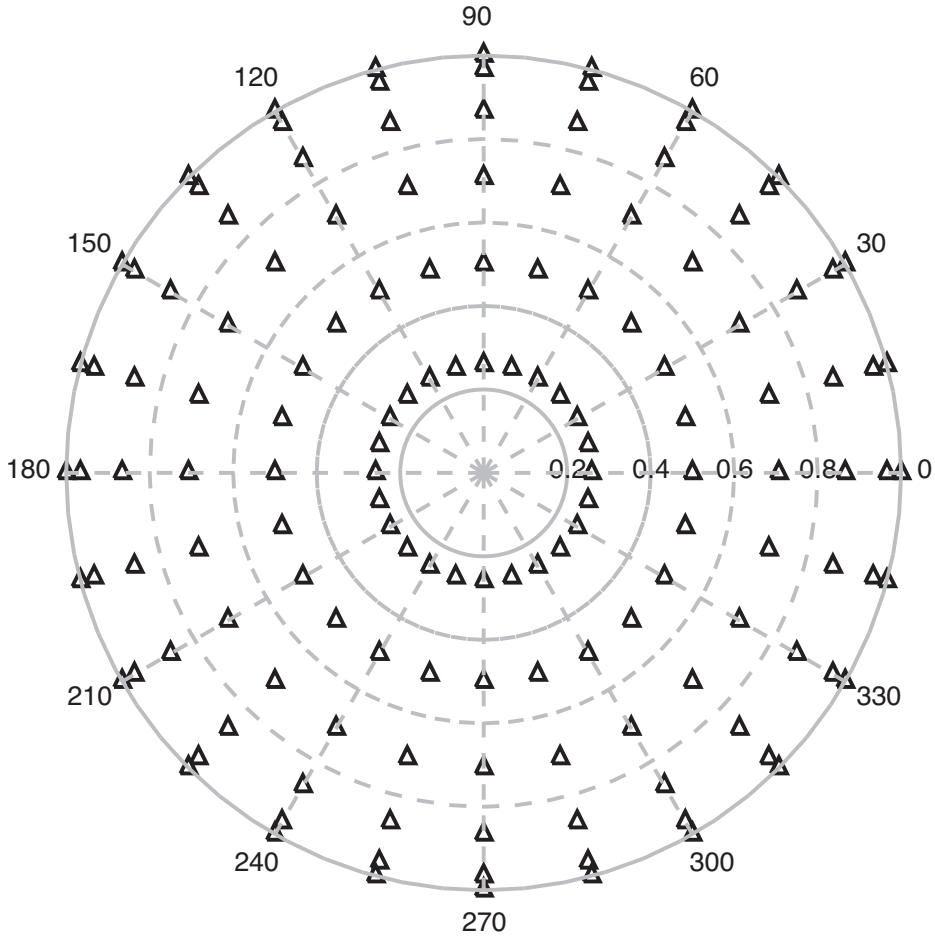

Figure 1. Distribution of diametrically situated sources and receivers on the surface of a spherical sample. Steps in azimuths and polar angles: 15°.

Table 1. 21 anisotropy parameters of the model used in the synthetic inversion experiment. *P*- and *S*-wave reference velocities are chosen $\alpha = 2.6\,\mathrm{km\,s^{-1}}$ and $\beta = 1.4\,\mathrm{km\,s^{-1}}$, *P*- and common *S*-wave anisotropy is ∼25 per cent and ∼21 per cent, respectively. Top: true values of parameters; middle: values estimated by inverting only *P*-wave traveltimes with random noise of 0.1 per cent (six empty spaces correspond to six *S*-wave parameters not evaluated in this experiment); bottom: values estimated by inverting *P*- and common *S*-wave travetimes with random noise of 0.2 per cent and 5 per cent, respectively.

Anisotropy Parameters	ϵ_x	ϵ_y	ϵ_z	χ_x	χ_y	χ_z	η_x
	η_y	η_z	ξ_{24}	ξ_{34}	ξ_{15}	ξ_{35}	ξ_{16}
	ξ_{26}	γ_x	γ_y	γ_z	ϵ_{45}	ϵ_{46}	ϵ_{56}
True	0.166	0.228	−0.061	0.	0.	0.	−0.220
	−0.299	−0.216	0.	0.	0.	0.	0.
	0.	0.010	−0.092	0.057	0.	0.	0.
Estimated P	0.151	0.212	−0.052	0.	0.001	0.	−0.293
	−0.346	−0.191	0.001	0.	0.	0.	0.
	0.001						
Estimated P+S	0.148	0.209	−0.054	−0.001	0.	−0.002	−0.281
	−0.333	−0.180	−0.001	−0.001	0.	0.	−0.0041
	−0.002	−0.032	−0.143	−0.007	−0.025	−0.010	−0.011

Synthetic data set

For the calculation of synthetic traveltimes, we use the two-point ray-tracing procedure of the program package ANRAY (Gajewski & Pšenčík 1990). It is important to mention that the used two-point ray-tracing procedure often results in more than two *S*-wave arrivals (*S*-wave ray-velocity surface is multivalued). We always choose the two fastest *S*-wave arrivals in such a case. As a model, we use a spherical sample of orthorhombic symmetry proposed by Schoenberg & Helbig (1997). The matrix of elastic moduli in Voigt notation is shown in eq. (C1) of Appendix C. For the corresponding anisotropy parameters, see Table 1, the box with true values. Symmetry planes of the orthorhombic medium coincide with coordinate planes. *P*- and common *S*-wave anisotropy strengths of the model are about 25 per cent and 20 per cent, respectively. The anisotropy of the model is intentionally chosen relatively strong to test the limits of the proposed procedure. The reference velocities α and β are chosen as $\alpha = 2.6\,\mathrm{km\,s^{-1}}$ and $\beta = 1.4\,\mathrm{km\,s^{-1}}$.

Laboratory data set

In the tests of the inversion of the laboratory data, sample sphere is used, which was prepared from a core segment of the Outokumpu scientific drill hole (Kukkonen 2011) recovered from 409 m depth (Kern *et al.* 2009). The sample sphere is 50 mm in diameter, with the bulk density of 2.72 g $\mathrm{cm^{-3}}$ (calculated from the mass and size of the sphere). The sample is a homogeneous biotite gneiss with pronounced foliation and lineation. The modal composition is 39.6 vol. per cent quartz, 36.9 vol. per cent plagioclase, 23.4 vol. per cent biotite, as determined by mass balance calculations (Kern *et al.* 2009). Foliation and lineation are defined by platy and elongated biotite minerals exhibiting strong shape-preferred orientation. The biotite grains are elongated subparallel to the lineation direction, ranging in length from 0.4 to 2 mm. The thickness of the biotite platelets perpendicular to foliation is about 5–300 μm. Quartz and plagioclase are more or less equiaxed with an average grain size of 0.1 mm. The platy biotite minerals are almost isolated and do not form compositional layers.

The equipment for the measurements consists of a pressure vessel connected to a two-step pressure generator, a sample positioning unit equipped with ultrasonic piezoceramic transducers allowing measurements of *P*- and *S*-wave waveforms on spherical samples with a diameter of 50 mm, and a device for generating ultrasonic pulses and traveltime measurement and data acquisition. For details, see Lokajíček & Svitek (2015). The sample can be exposed to hydrostatic pressures ranging from 0.1 up to 100 MPa. The signals are excited and recorded by three piezoceramic sensor pairs with resonant frequency of 2 MHz and 700 kHz for longitudinal and shear polarization, respectively.

Due to the good quality of first *P*-wave onsets, an automatic algorithm to determine *P*-wave arrival time is used (Svitek *et al.* 2010). The first arrivals of S1 (fast) and S2 (slow) wave are more complex; thus, they are determined manually by an operator.

INVERSION TESTS

In the following tests, we make two types of inversion. First, we invert only *P*-wave traveltime data using a system of 132 equations resulting from formula (2). The inversion yields, in this case, 15 anisotropy parameters sufficient for the approximate reconstruction of the *P*-wave phase-velocity surface. Secondly, we invert both *P*- and common *S*-wave traveltimes using a system of 264 equations resulting from formulae (2) and (3) to obtain the complete set of 21 anisotropy parameters. In both cases, the solved system of equations is strongly overdetermined. In case of the inversion of *P*-wave traveltimes only, parameters γ_x, γ_y, γ_z, ϵ_{45}, ϵ_{46} and ϵ_{56} are formally set equal zero. Anisotropy parameters are ordered as indicated in eq. (9) or Tables 1 and 2.

For each of the following tests, we show model covariance matrices determined in the way described in Appendix A. Usually, model covariance matrix is reflecting data randomness transformed to randomness of model parameters. However, we deal with deterministic, not random data, which are, however, inexact due to the approximate character of used eqs (2) and (3). Thus, covariance matrix can be formally constructed in the same way as from the data with random noise. The following experiments are, therefore, discussed uniquely in

terms of model covariance matrices. Besides covariance matrices, we also show estimated anisotropy parameters and phase-velocity surfaces reconstructed from the true and estimated anisotropy parameters using eqs (2) and (3). The colours in covariance matrices indicate positive (red) or negative (blue) deviations from zero. The colour corresponding to zero is white. The non-negative values of the diagonal elements represent variances of corresponding anisotropy parameters. Their square roots are used for the determination of the size of error bars in the plots of anisotropy parameters. The non-zero values of off-diagonal elements indicate correlation between corresponding parameters. In the plots of anisotropy parameters, we show the true values by open black circles and estimated values by red squares. The error bars are blue. The intervals limited by the error bars include, approximately, the true solution with 99.7 per cent probability.

Inversion of synthetic data

Fig. 2 shows the covariance matrices related to the inversion of *P*-wave traveltimes only (top) and the covariance matrix related to the inversion of both *P*- and common *S*-wave traveltimes (bottom). The traveltimes are inverted with no noise added. One can see that only variations of anisotropy parameters ϵ can be considered effectively zero for the chosen scale. Variations of all remaining parameters are non-zero. The parameters with largest variations (red) are η parameters, η_z having strongest variations. The upper plot of Fig. 2 also indicates the correlation between individual anisotropy parameters. For example, we can see that parameters ξ are positively correlated with parameters χ.

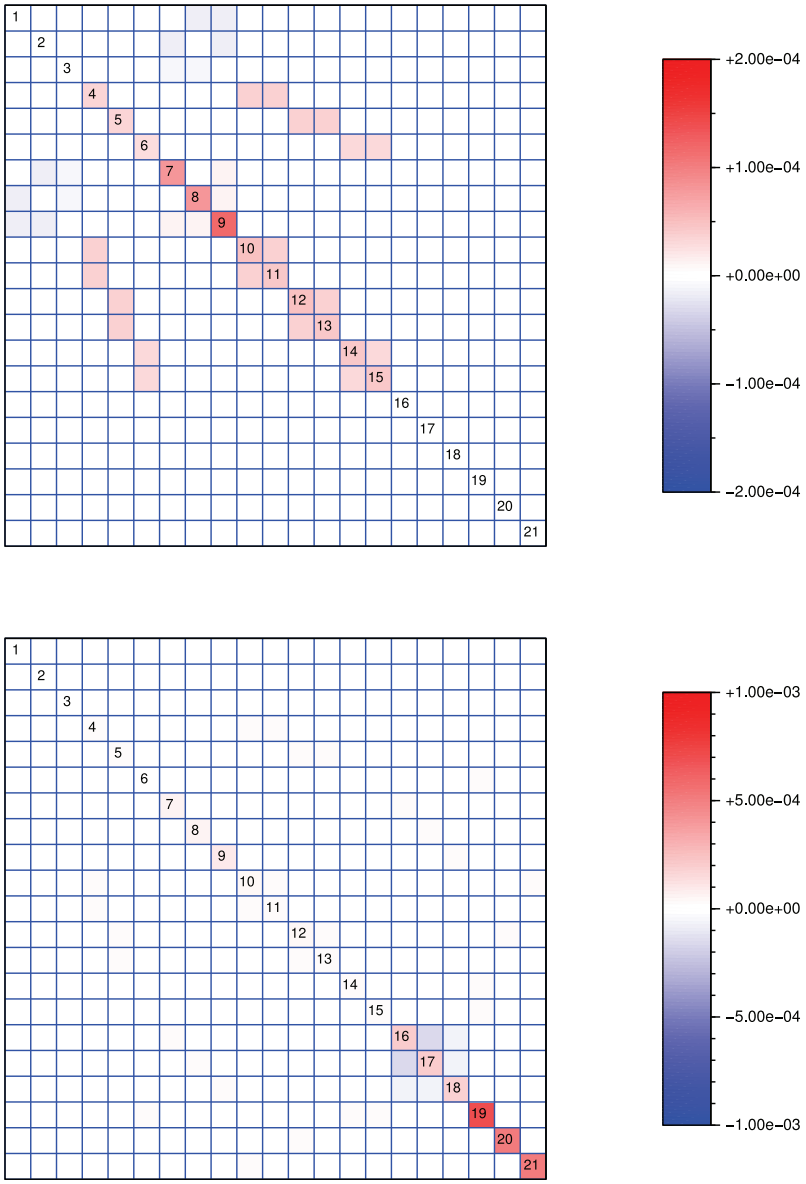

Figure 2. Covariance matrices related to the inversion of synthetic traveltimes with no noise. Top: *P*-wave traveltimes alone used. Bottom: *P*- and common *S*-wave traveltimes used together. Colours indicate non-zero values of the elements of the covariance matrix. Note the difference in scales in the top and bottom plots. Anisotropy parameters are ordered as indicated in eq. (9).

Consideration of common *S*-wave traveltimes in addition to *P*-wave traveltimes allows to estimate 6 remaining anisotropy parameters related to *S* waves. The part of the covariance matrix related to 15 anisotropy parameters shown in the upper plot of Fig. 2 remains effectively unchanged. Use of *S*-wave traveltimes does not affect it. The variances of the 6 remaining parameters are, however, so large that they require change of the scale by nearly one order. We can observe especially large variances of parameters ϵ_{45}, ϵ_{46} and ϵ_{56}. Variations of γ parameters are slightly weaker, parameters γ_x and γ_y are weakly negatively correlated.

The observations based on the behaviour of covariance matrices are reflected in Fig. 3, which shows comparison of true and estimated anisotropy parameters from the inversion of *P*-wave only (top) and *P*- and common *S*-wave (bottom) noiseless traveltimes. In the top plot we can see that except parameters η, whose true and estimated values slightly differ, the fit of remaining estimated and true anisotropy parameters is very good. In the bottom plot we can see that addition of common *S*-wave traveltimes makes possible the estimation of *S*-wave anisotropy parameters, and brings effectively no observable improvement of parameters estimated by the inversion of separate *P*-wave traveltimes. Generally, variances of *S*-wave anisotropy parameters are larger. Although variances of parameters ϵ_{45}, ϵ_{46} and ϵ_{56} exceed variances of parameters γ, they are estimated more accurately than parameters γ, especially γ_y and γ_z. We discuss this phenomenon in the concluding section.

In Fig. 4, we show effects of random Gaussian noise added to the *P*- and common *S*-wave traveltimes. In the top plot, the noise added to *P*-wave traveltimes represents 0.2 per cent of averaged *P*-wave traveltimes, the noise added to common *S*-wave traveltimes represents 5 per cent

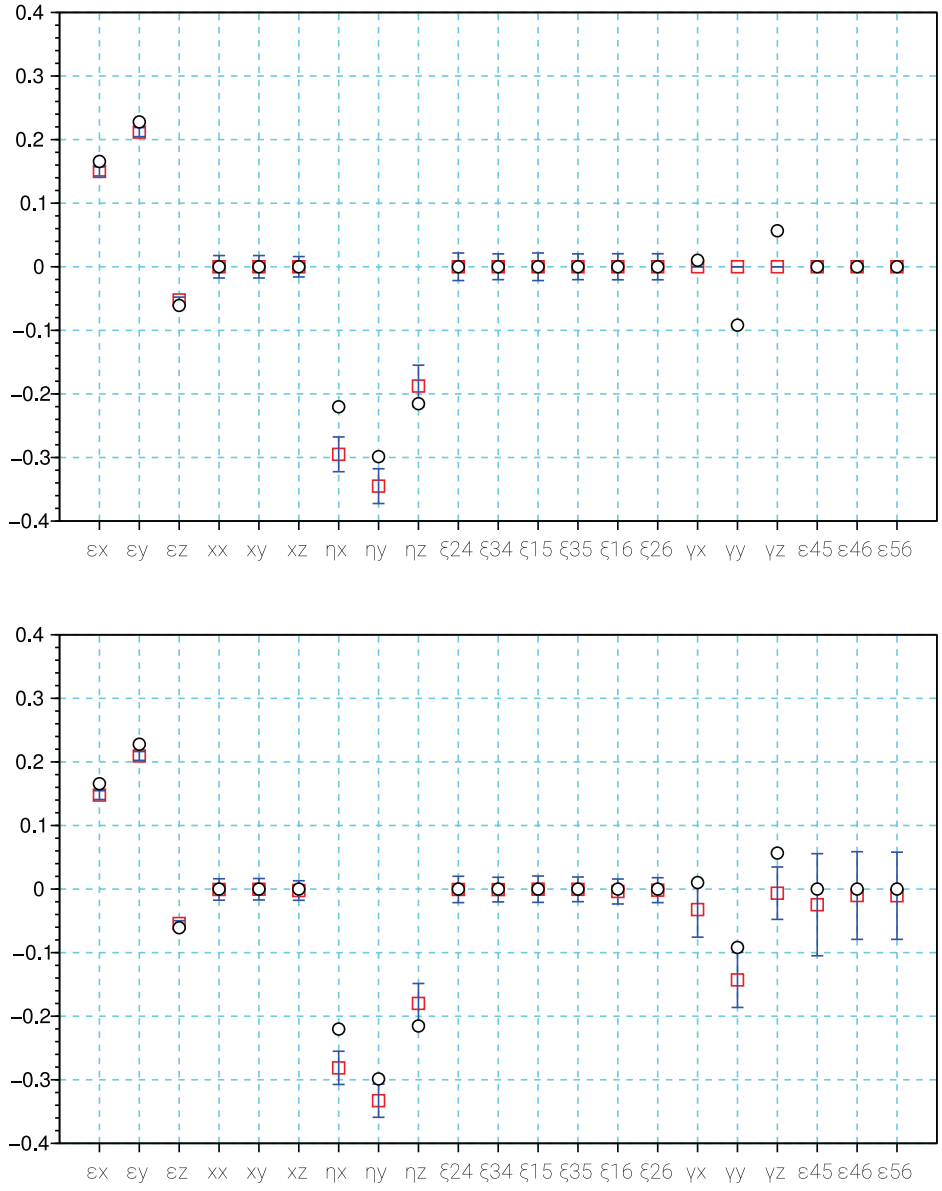

Figure 3. Results of the inversion of synthetic data with no noise. Top: anisotropy parameters estimated from *P*-wave traveltimes only through eq. (2); bottom: parameters estimated from *P*- and common *S*-wave traveltimes through eqs (2) and (3). Black circles: true values, red squares: inverted parameters, blue lines: error bars. Reference velocities: $\alpha = 2.6\,\mathrm{km\,s^{-1}}$ and $\beta = 1.4\,\mathrm{km\,s^{-1}}$.

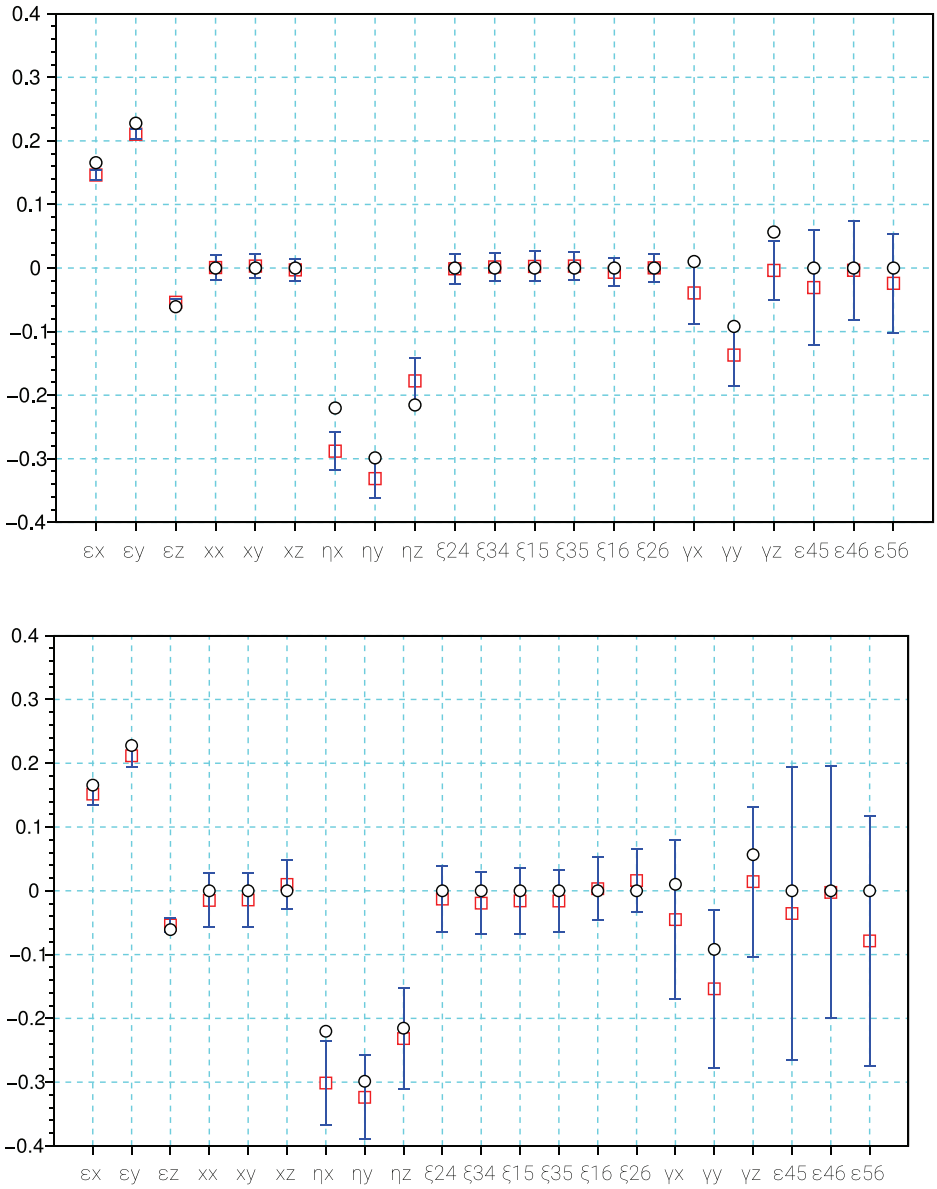

Figure 4. Results of the inversion of synthetic data with random Gaussian noise of 0.2 per cent and 5 per cent (top) and 1 per cent and 10 per cent (bottom) added to *P*- and common *S*-wave traveltimes, respectively. Anisotropy parameters estimated from *P*- and common *S*-wave traveltimes through eqs (2) and (3). Black circles: true values, red squares: inverted parameters, blue lines: error bars. Reference velocities: $\alpha = 2.6\,\mathrm{km\,s^{-1}}$ and $\beta = 1.4\,\mathrm{km\,s^{-1}}$.

of averaged *S*-wave traveltimes. It is interesting to see that the introduction of noise has no observable effect on inverted parameters. Only error bars increase correspondingly. The same can be seen in the bottom plot, in which the noise added to *P*-wave traveltimes is 1 per cent and to common *S*-wave traveltimes is 10 per cent.

The true and estimated anisotropy parameters can be used in the construction of approximate *P*-wave and common *S*-wave velocity surfaces, see Figs 5 and 6.

All the surfaces in Fig. 5 are approximate *P*-wave velocity surfaces calculated from eq. (2) for three sets of anisotropy parameters. In the top plot of Fig. 5, the true parameters shown in the top box of Table 1 are used. The top plot thus represents a kind of a reference for the two remaining plots. The middle plot in Fig. 5 is obtained by using anisotropy parameters obtained from the inversion of *P*-wave traveltimes alone with random noise of 0.2 per cent, see the top plot in Fig. 4 and the values shown in the middle box of Table 1. The bottom plot is obtained by using anisotropy parameters obtained from the inversion of both *P*- and *S*-wave traveltime data with random noise of 0.2 per cent for *P* wave and 5 per cent for common *S* wave. See the top plot of Fig. 4 again and values given in the bottom box of Table 1. By comparing the middle and bottom plots of Fig. 5 with the plot at the top, we can conclude that the estimated parameters, despite the errors present in the top plot of Fig. 4, allow highly accurate reconstruction of the approximate *P*-wave velocity surface. The additional use of *S*-wave traveltimes does not seem to have observable effect, compare middle and bottom plots of Fig. 5.

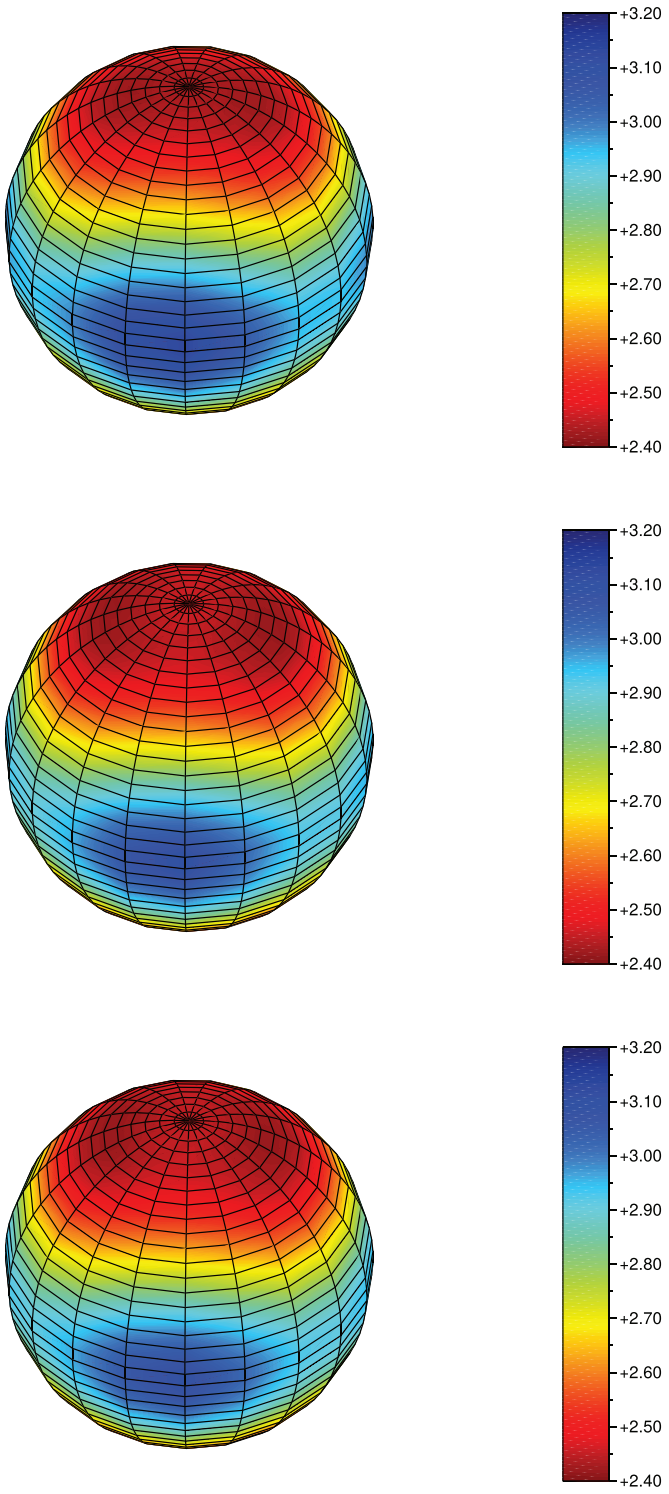

Figure 5. *P*-wave velocity surfaces calculated from eq. (2). Exact anisotropy parameters (top), parameters estimated from *P*-wave traveltimes only with 0.2 per cent noise (middle) and anisotropy parameters estimated from *P*- and common *S*-wave traveltimes with random noise of 0.2 per cent and 5 per cent (bottom) used, respectively.

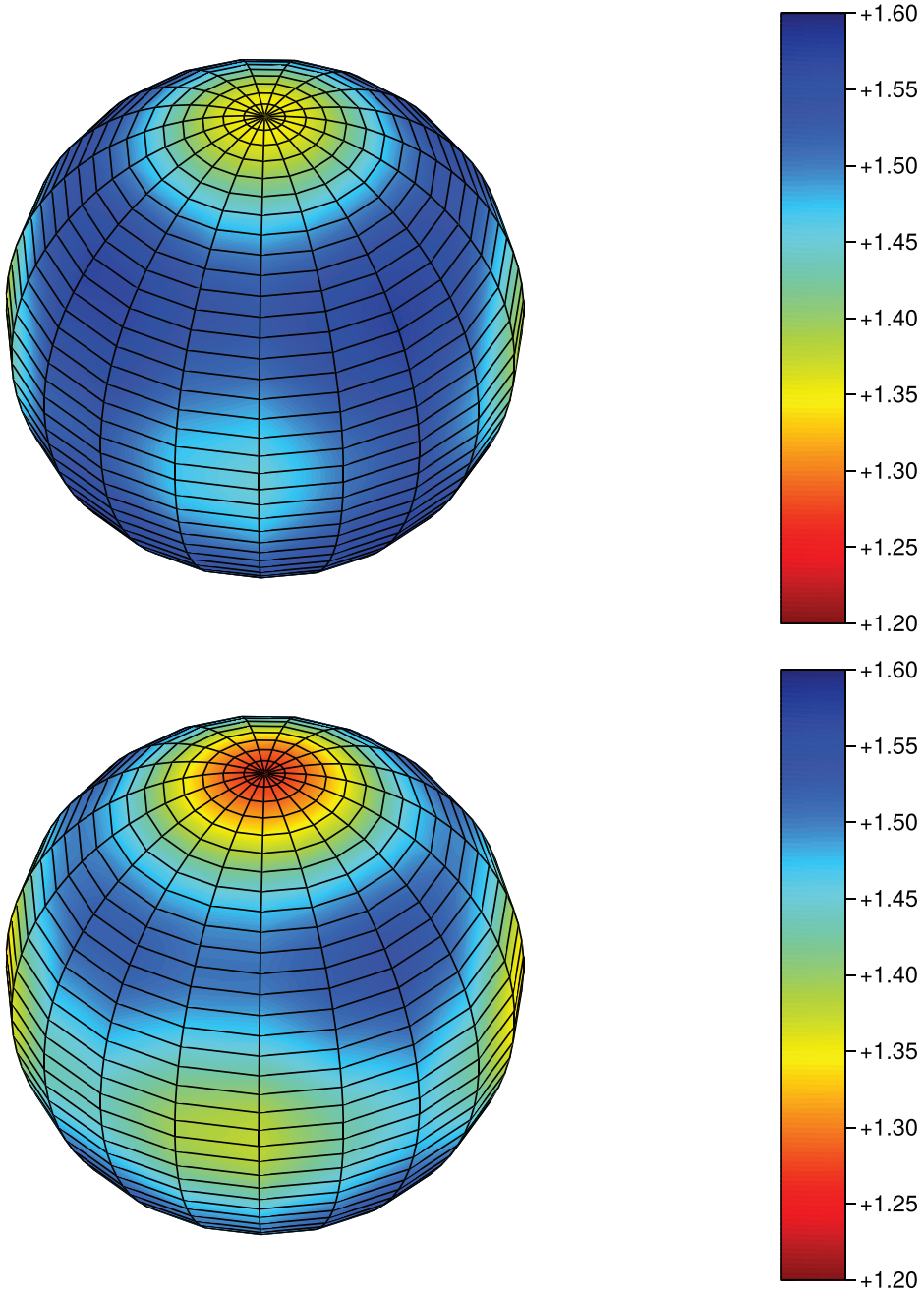

Figure 6. Common *S*-wave velocity surfaces calculated from eq. (3). Exact anisotropy parameters (top) and parameters estimated from *P*- and common *S*-wave traveltimes with random noise of 0.2 per cent and 5 per cent (bottom) used, respectively.

In Fig. 6, common *S*-wave velocity surfaces calculated from eq. (3) for two sets of anisotropy parameters are shown. The top plot is obtained from true parameters shown in the top box of Table 1. The bottom plot of Fig. 6 is obtained from parameters found by the inversion of *P*- and *S*-wave traveltimes with random Gaussian noise of 0.2 per cent and 5 per cent added to *P*- and *S*-wave traveltimes, respectively. One can see that the fit of plots is worse than in the case of *P* waves. Nevertheless, coincidence of positions of local minima and maxima of common *S*-wave velocity surface can be clearly identified.

Inversion of laboratory data

As with synthetic data, in the first test we use eq. (2) alone for the inversion, that is, we invert *P*-wave traveltimes alone. In the next step, we use eqs (2) and (3) for the inversion of both *P*- and *S*-wave traveltimes. Covariance matrices for the former and latter tests are shown in the top and bottom plots of Fig. 7, respectively. The covariance matrix corresponding to the inversion of *P*-wave traveltimes alone has a similar character to the corresponding covariance matrix in Fig. 2. Thanks to the use of lower values in the scale of the top plot of Fig. 7 than in

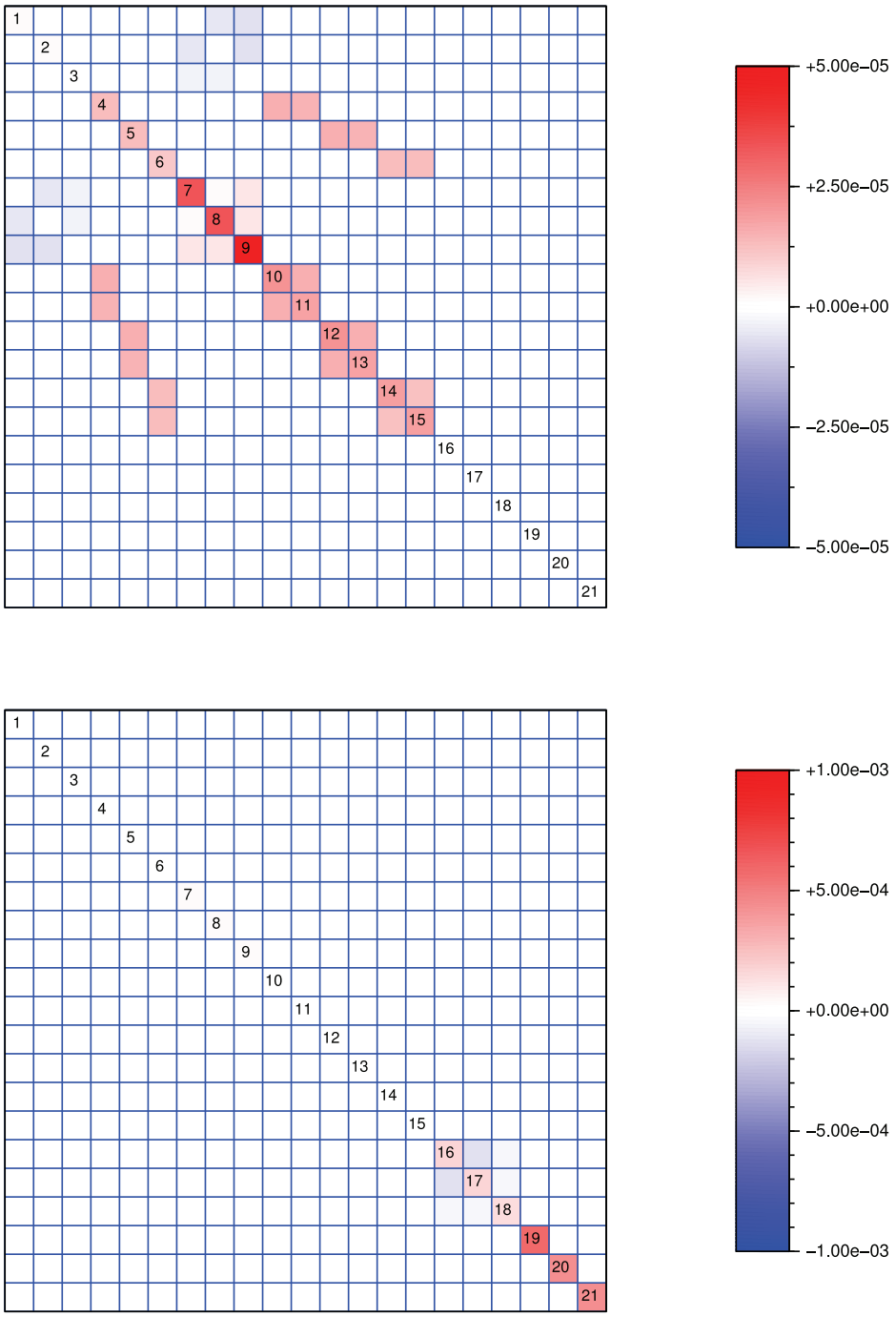

Figure 7. Covariance matrices related to the inversion of laboratory traveltimes. Top: *P*-wave traveltimes alone used to invert eq. (2); bottom: *P*- and common *S*-wave traveltimes used to invert eqs (2) and (3). Colours indicate non-zero values of the elements of the covariance matrix. Note the difference in scales in the top and bottom plots. Anisotropy parameters are ordered as indicated in eq. (9).

Fig. 2, the variances and correlations are more pronounced and the plot also indicates a weak correlation of η parameters with ϵ parameters. As in the synthetic test, the covariance matrix in the bottom plot, in which *P*- and *S*-wave traveltimes are used, indicates that γ parameters have considerably smaller variances than parameters ϵ_{45}, ϵ_{46} and ϵ_{56}. Note that the scale in the bottom plot differs significantly from the scale in the upper plot. *P*- and common *S*-wave anisotropy is estimated to be about 20 per cent and 13 per cent, respectively.

In the upper plot of Fig. 8, one can see *P*-wave anisotropy parameters estimated from *P*-wave traveltimes alone, inverted using eq. (2). As in synthetic tests, variances of ϵ parameters are considerably smaller than variances of remaining involved anisotropy parameters. This remains the same in the bottom plot of Fig. 8, obtained by the inversion of both *P*- and *S*-wave traveltimes using both eqs (2) and (3). Variances corresponding to six *S*-wave anisotropy parameters, especially of ϵ_{45}, ϵ_{46} and ϵ_{56}, indicate that the determination of these parameters is less accurate. Values of parameters found in both inversion tests are given in Table 2.

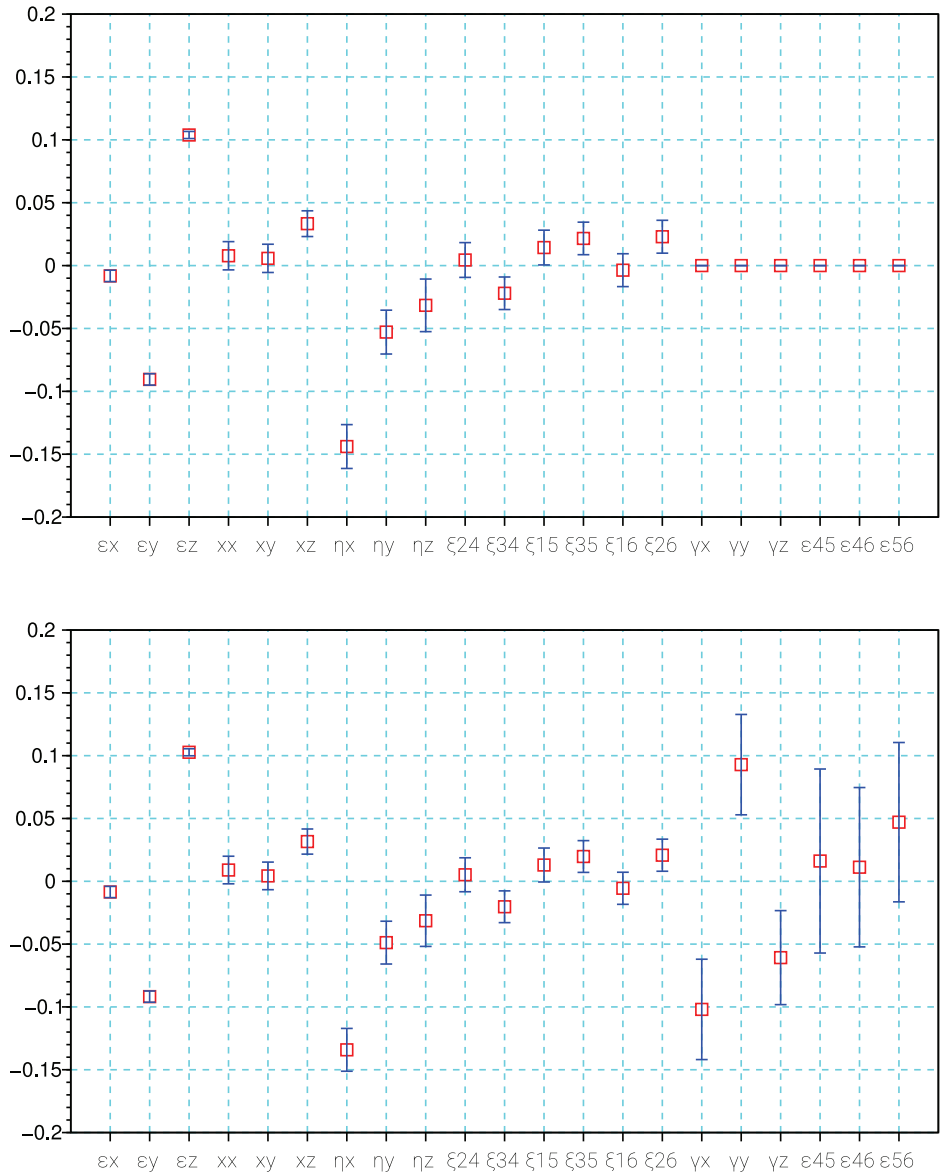

Figure 8. Results of the inversion of laboratory traveltimes. Anisotropy parameters estimated from only *P*-wave traveltimes through eq. (2) (top); from *P*- and common *S*-wave traveltimes through eqs (2) and (3) (bottom). Black circles: true values, red squares: inverted parameters, blue lines: error bars. Reference velocities: $\alpha = 5.5\,\mathrm{km\,s^{-1}}$ and $\beta = 3.0\,\mathrm{km\,s^{-1}}$.

Table 2. 21 anisotropy parameters determined by inverting laboratory data. *P*- and *S*-wave reference velocities chosen as $\alpha = 5.5\,\mathrm{km\,s^{-1}}$ and $\beta = 3.0\,\mathrm{km\,s^{-1}}$. Estimated *P*- and common *S*-wave anisotropy is ∼20 per cent and ∼13 per cent, respectively. Top: values estimated by inverting *P*-wave traveltimes only (six empty spaces correspond to six *S*-wave parameters not evaluated in this experiment); bottom: values estimated by inverting *P*- and common *S*-wave traveltimes together.

Anisotropy Parameters	ϵ_x	ϵ_y	ϵ_z	χ_x	χ_y	χ_z	η_x
	η_y	η_z	ξ_{24}	ξ_{34}	ξ_{15}	ξ_{35}	ξ_{16}
	ξ_{26}	γ_x	γ_y	γ_z	ϵ_{45}	ϵ_{46}	ϵ_{56}
Estimated P	−0.008	−0.091	0.104	0.008	0.006	0.033	−0.144
	−0.053	0.032	0.005	0.022	0.014	0.022	−0.004
	0.023						
Estimated P + S	−0.009	−0.092	0.103	0.009	0.004	0.032	−0.134
	−0.049	−0.031	0.005	−0.020	0.013	0.020	−0.006
	0.021	−0.102	0.093	−0.061	0.016	0.011	0.047

In Fig. 9, *P*-wave velocity surface determined from eq. (2) (top and middle plots) and common *S*-wave velocity surface determined from eq. (3) (bottom) are shown. *P*-wave surfaces are calculated from anisotropy parameters obtained by the inversion of *P*-wave traveltimes alone (top) and from both *P*- and *S*-wave traveltimes (middle). The bottom plot represents common *S*-wave velocity surface and is constructed from anisotropy parameters obtained by the inversion of *P*- and *S*-wave traveltimes.

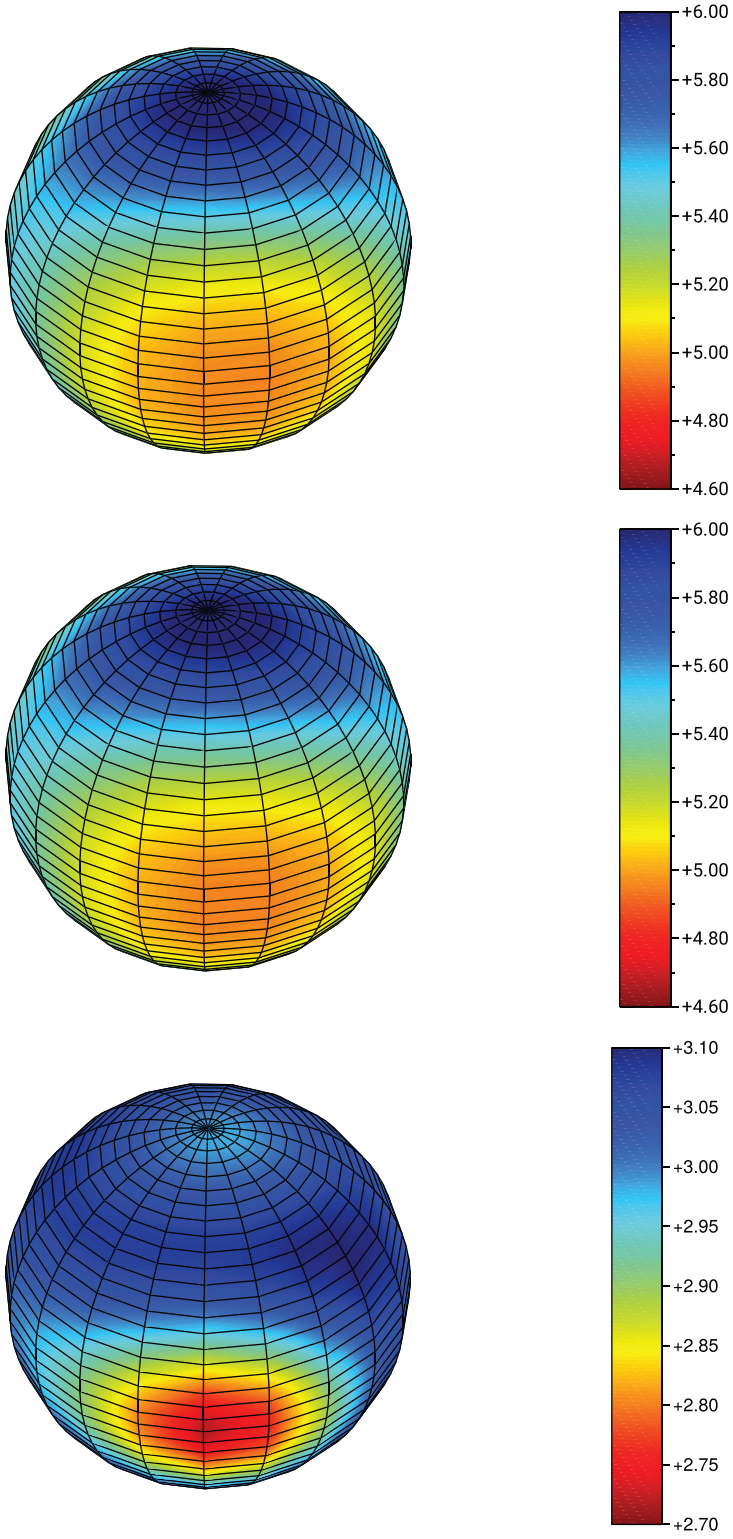

Figure 9. *P*-wave velocity surfaces calculated from eq. (2) (top and middle) and common *S*-wave velocity surface calculated from eq. (3) (bottom). Anisotropy parameters estimated by inverting only eq. (2) (top) and parameters estimated by inverting eqs (2) and (3) together (middle and bottom). Estimated *P*- and common *S*-wave anisotropy is $\sim$ 20 per cent and 13 per cent, respectively.

The plots, especially those obtained from the *P*-wave traveltimes, indicate that the medium is of orthorhombic symmetry with one nearly vertical symmetry plane deviating slightly from the (x_1, x_3) coordinate plane. It is in agreement with the description given by Svitek *et al.* (2014) and Lokajíček *et al.* (2014). Inversion of 3-D experimental data confirms petrographic thin section analysis, which showed crystallographic and shape-preferred orientation of the biotite minerals. The observed data are available upon a request.

DISCUSSION AND CONCLUSIONS

We proposed an inversion scheme based on several useful alternative concepts. We made no *a priori* assumption about the type of the anisotropy and seek the complete set of parameters specifying it. With the inversion scheme, we were able to recover the complete set of parameters specifying a general anisotropic medium from available *P*- and *S*-wave traveltimes. The tests performed in this paper indicate that with the *P*-wave traveltimes alone, it is possible to reconstruct the *P*-wave velocity surface with a high accuracy. Additional use of *S*-wave traveltimes leads to the completion of the set of parameters specifying the medium, it does not seem, however, to affect very much the parameters estimated from *P*-wave traveltimes alone. The inverted parameters allow reconstruction of common *S*-wave velocity surface, but with a lower accuracy than in the case of *P* waves. Anisotropy parameters found from the joint inversion of *P*- and *S*-wave traveltimes can be, in principle, used for the construction of *P*, *S*1- and *S*2-wave phase- and ray-velocity surfaces, calculated from exact or approximate expressions. Such surfaces can be used for the estimate of the type of anisotropy and its orientation.

The inversion scheme is based on simple, linear (with respect to the parameters of the medium) approximate formulae for squares of *P*-wave and common *S*-wave velocities to estimate anisotropy of spherical rock samples from the measured traveltimes. For the parametrization of the medium, we used anisotropy parameters (1).

The tested approach has several advantages when compared with traditionally used approaches. The used anisotropy parameters take into account combinations of elastic moduli in the Voigt notation (see eq. 1), which, if considered separately, complicate the inversion. The use of anisotropy parameters in the combination with the weak-anisotropy approximation allows to deal with *P* and *S* waves separately. *P* and common *S* waves are described each by 15 parameters instead of 21 parameters in the Voigt notation.

Important advantage of the proposed approach is the use of the weak-anisotropy approximation, within which the ray and phase velocity vectors are assumed to be identical. Actually, these vectors may differ, especially in their direction, quite significantly, see, for example, Farra *et al.* (2016). However, as we have shown in our previous studies (Růžek & Pšenčík 2016), in the presence of noise, the used approximation is sufficiently accurate for the inversion purposes. We thus do not need to care whether the measured velocities are ray or phase velocities, which was the problem of inversion schemes based on exact equations, see, for example, Dellinger & Vernik (1994) or Vestrum (1994).

Another useful advantage of the proposed approach is the use of the so-called common *S* wave (Farra & Pšenčík 2008; Pšenčík *et al.*, 2012) instead of two separate *S* waves propagating in anisotropic media. We thus do not need to identify individual *S* waves, which simplifies considerably the inversion process.

The remaining problem connected with the use of *S*-wave traveltimes, which still requires an additional study, is the multivaluedness of the traveltimes. As mentioned in the text, in synthetic and laboratory data, we always used the first two fastest *S*-wave arrivals for the inversion. In directions, in which one can observe more than two *S*-wave arrivals, this might not be the best choice. This, together with the fact that eqs (2) and (3) yield systematically lower and higher values than exact, probably causes considerably larger variations and sometimes deviations from the intervals specified by the error bars of estimated parameters. Additional synthetic tests are necessary to confirm or rebut the above doubts.

ACKNOWLEDGEMENTS

We appreciate comments of Einar Iversen, Faranak Mahmoudian and an anonymous referee, which helped us to improve the original text. We are grateful to the Research Project 16-05237S and partly 16-03950S of the Grant Agency of the Czech Republic, the research project of the Czech Academy of Sciences, RVO 67985831 and the project 'Seismic waves in complex 3-D structures' (SW3D) for support.

REFERENCES

Alkhalifah, T. & Tsvankin, I., 1995. Velocity analysis for transversely isotropic media, *Geophysics,* **60,** 1550–1566.

Arts, R.J., 1993. A study of general anisotropic elasticity in rocks by wave propagation: theoretical and experimental aspects, *PhD thesis,* Institut Français du Pétrole.

Arts, R.J., Rasolofosaon, N.J.P. & Zinszner, B.E., 1991. Complete inversion of the anisotropic elastic tensor in rocks: experiment versus theory, in *Proceedings of the 61st Annual International Meeting, SEG, Expanded Abstracts,* 1538–1540.

Aster, R.C., Borchers, B. & Thurber, C.H., 2005. *Parameter Estimation and Inverse Problems,* Elsevier.

Dellinger, J. & Vernik, L., 1994. Do traveltimes in pulse-transmission experiments yield anisotropic group or phase velocities? *Geophysics,* **59,** 1774–1779.

Farra, V. & Pšenčík, I., 2003. Properties of the zero-, first- and higher-order approximations of attributes of elastic waves in weakly anisotropic media, *J. acoust. Soc. Am.,* **114,** 1366–1378.

Farra, V. & Pšenčík, I., 2008. First-order ray computations of coupled S waves in inhomogeneous weakly anisotropic media, *Geophys. J. Int.,* **173,** 979–989.

Farra, V. & Pšenčík, I., 2016. Weak-anisotropy approximations of P-wave phase and ray velocities for anisotropy of arbitrary symmetry, *Stud. Geophys. Geod.,* **60,** 403–418.

Farra, V., Pšenčík, I. & Jílek, P., 2016. Weak-anisotropy moveout approximations for P waves in homogeneous layers of monoclinic or higher anisotropy symmetries, *Geophysics,* **81,** C39–C59.

Gajewski, D. & Pšenčík, I., 1990. Vertical seismic profile synthetics by dynamic ray tracing in laterally varying layered anisotropic structures, *J. geophys. Res.,* **95,** 11 301–11 315.

Grechka, V., 2017. Algebraic degree of a general group-velocity surface, *Geophysics,* **83,** WA45–WA53.

Jech, J., 1991. Computation of elastic parameters of anisotropic medium from traveltimes of quasi-compressional waves, *Phys. Earth planet. Inter.,* **66,** 153–159.

Kern, H., Mengel, K., Strauss, K.W., Ivankina, T.I., Nikitin, A.N. & Kukkonen, I., 2009. Elastic wave velocities, chemistry and modal mineralogy of crustal rocks sampled by the Outokumpu scientific drill hole: evidence from lab measurements and modeling, *Phys. Earth planet. Inter.,* **175,** 151–166.

Kukkonen, I., 2011. *Outokumpu Deep Drilling Project 2003-2010,* Vol. **51,** of Special Paper, Geological Survey of Finland, pp. 252.

Lokajíček, T. & Svitek, T., 2015. Laboratory measurement of elastic anisotropy on spherical rock samples by longitudinal and transverse sounding under confining pressure, *Ultrasonics,* **56,** 294–302.

Lokajíček, T., Kern, H., Svitek, T. & Ivankina, T., 2014. 3D velocity distribution of P- and S-waves in a biotite gneiss, measured in oil as the pressure medium: comparison with velocity measurements in a multi-anvil pressure apparatus and with texture-based calculated data, *Phys. Earth planet. Inter.,* **231,** 1–15.

Mahmoudian, F., Margrave, G.F., Daley, P.F., Wong, J. & Henley, D.C., 2014. Estimation of elastic stiffness coefficients of an orthorhombic physical model using group velocity analysis on transmission data, *Geophysics,* **79,** R27–R39.

Mensch, T. & Rasolofosaon, P., 1997. Elastic wave velocities in anisotropic media of arbitrary anisotropy–generalization of Thomsen's parameters ϵ, δ and γ, *Geophys. J. Int.,* **128,** 43–64.

Pšenčík, I. & Gajewski, D., 1998. Polarization, phase velocity and NMO velocity of *qP* waves in arbitrary weakly anisotropic media, *Geophysics,* **63,** 1754–1766.

Pšenčík, I., Farra, V. & Tessmer, E., 2012. Comparison of the FORT approximation of the coupling ray theory with the Fourier pseudospectral method, *Stud. Geophys. Geod.,* **56,** 35–64.

Pšenčík, I., Růžek, B., Lokajíček, T. & Svitek, T., 2017. Determination of rock-sample anisotropy from P- and S-wave traveltimes, *Seismic waves in complex 3-D structures,* 27, 15–35, Available at:. http://sw3d.cz, last accessed 1 January 2018.

Růžek , B. & Pšenčík, I., 2016. P-wave VSP traveltime inversion in weakly and moderately anisotropic media, *Seismic waves in complex 3-D structures,* 26, 17–59. Availabe at: http://sw3d.cz, last accessed 1 January 2017.

Schoenberg, M. & Helbig, K., 1997. Orthorhombic media: modeling elastic wave behavior in a vertically fractured earth, *Geophysics,* **62,** 1954–1974.

Svitek, T., Rudajev, V. & Petružálek, M., 2010. Determination of P-wave arrival time of acoustic events, *Acta Montan. Slov.,* **15,** 145–151.

Svitek, T., Vavryčuk, V., Lokajíček, T. & Petružálek, M., 2014. Determination of elastic anisotropy of rocks from P- and S-wave velocities: numerical modelling and lab measurements, *Geophys. J. Int.,* **199,** 1682–1697.

Thomsen, L., 1986. Weak elastic anisotropy, *Geophysics,* **51,** 1954–1966.

Tsvankin, I. & Grechka, V., 2011. *Seismology of Azimuthally Anisotropic Media and Seismic Fracture Characterization,* Society of Exploration Geophysicists.

Vestrum, R.W., 1994. Group- and phase-velocity inversions for the general anisotropic stiffness tensor, *PhD thesis,* The University of Calgary.

APPENDIX A: MODEL COVARIANCE MATRIX AND ERRORS OF MODEL PARAMETERS

The simplest way how to asses the model parameters' uncertainties is to transform the data covariance matrix $\mathbf{C}_d$ to the model covariance matrix $\mathbf{C}_m$:

$$\mathbf{C}_m = \mathbf{H}\mathbf{C}_d\mathbf{H}^T, \tag{A1}$$

where $\mathbf{H} = \mathbf{G}^\dagger$. Here, $\mathbf{G}^\dagger$ denotes pseudoinverse of $\mathbf{G}$. The model covariance matrix $\mathbf{C}_m$ describes, approximately, the probability distribution of the random vector of model parameters $\mathbf{m}$. In an ideal case, with no randomness, the covariance matrix is zero, indicating error-less vector $\mathbf{m}$. Diagonal elements of matrix $\mathbf{C}_m$ are variances of individual anisotropy parameters, off-diagonal elements are covariances describing relations between various components of vector $\mathbf{m}$. Square roots of diagonal elements of $\mathbf{C}_m$ are standard deviations of individual components of $\mathbf{m}$. Positive (negative) off-diagonal elements of the covariance matrix $\mathbf{C}_m$ indicate positive (negative) correlation of the corresponding components of $\mathbf{m}$. Zero off-diagonal elements of $\mathbf{C}_m$ indicate independent component pair.

If we do not know the data covariance matrix $\mathbf{C}_d$ exactly, which is the case of laboratory data, we use its approximation in the following form:

$$\mathbf{C}_d \sim \sigma^2\mathbf{I}. \tag{A2}$$

The factor σ is determined using χ^2 statistics of residuals

$$\mathbf{r} = \mathbf{d} - \mathbf{G}\tilde{\mathbf{m}}, \tag{A3}$$

with the degree of freedom ν (number of equations of the system minus number of sought parameters):

$$\sigma = \sqrt{\frac{\mathbf{r}^T\mathbf{r}}{\nu}}. \tag{A4}$$

The symbol $\tilde{\mathbf{m}}$ in eq. (A3) denotes the solution of eq. (6) obtained using the pseudoinverse $\mathbf{G}^\dagger$ of $\mathbf{G}$, $\tilde{\mathbf{m}} = \mathbf{G}^\dagger\mathbf{d}$. Eq. (A4) results from the approximate relation

$$\nu^{-1}\mathbf{r}^T\mathbf{C}_d^{-1}\mathbf{r} = \nu^{-1}\frac{\mathbf{r}^T\mathbf{r}}{\sigma^2} \sim 1. \tag{A5}$$

Applying eqs (A1)–(A5) to the system of equations containing both *P* and *S*-wave traveltimes, components of the residual vector $\mathbf{r}_S$ corresponding to *S* waves have usually different absolute values than components of residual vector $\mathbf{r}_P$ of *P* waves. This is because *S*-wave

traveltimes have usually different errors than *P*-wave traveltimes, eqs (2) and (3) have different accuracy, etc. To compensate this effect, individual weighting of equations for *P* and *S* waves is necessary. Therefore, we replace the relation (A2) by

$$\mathbf{C}_d \sim \sigma^2 \begin{pmatrix} \mathbf{I_P} & \mathbf{0} \\ \mathbf{0} & \lambda^2 \mathbf{I}_S \end{pmatrix}. \tag{A6}$$

Here, $\mathbf{I}_P$ and $\mathbf{I}_S$ are identity matrices corresponding to *P*- and *S*-wave traveltimes, respectively. The parameter λ is the weighting factor

$$\lambda = |\mathbf{r}_S|/|\mathbf{r}_P|, \tag{A7}$$

which is sought numerically. The symbols $|\mathbf{r}_P|$ and $|\mathbf{r}_S|$ denote the L2-norm of vectors $\mathbf{r}_P$ and $\mathbf{r}_S$, respectively.

Taking into account the above relations, the model covariance matrix $\mathbf{C}_m$ attains the final approximate form:

$$\mathbf{C}_m \sim \sigma^2 \mathbf{H} \begin{pmatrix} \mathbf{I_P} & \mathbf{0} \\ \mathbf{0} & \lambda^2 \mathbf{I}_S \end{pmatrix} \mathbf{H}^T. \tag{A8}$$

APPENDIX B: MAXIMUM LIKELIHOOD SOLUTION OF THE SYSTEM OF LINEAR EQUATIONS

Straightforward solution of eq. (6) does not account for different precission of individual equations. As a rule the *S*-wave-related equations are of lower accuracy than the *P*-wave-related equations. In order to solve properly the well-balanced system of equations, maximum likelihood principle can be used (e.g. Aster *et al.* 2005), which results in solving weighted system:

$$\mathbf{G}'\mathbf{m} = \mathbf{d}'. \tag{B1}$$

In eq. (B1), $\mathbf{G}' = \mathbf{QG}$ and $\mathbf{d}' = \mathbf{Qd}$, where the weighting matrix $\mathbf{Q}$, whose square is the inverse of the matrix $\mathbf{C}_d$, reads

$$\mathbf{Q} = \sigma^{-1} \begin{pmatrix} \mathbf{I_P} & \mathbf{0} \\ \mathbf{0} & \lambda^{-1} \mathbf{I}_S \end{pmatrix}. \tag{B2}$$

Eq. (B1) is thus the error-weighted version of eq. (6).

APPENDIX C: THE DENSITY-NORMALIZED ELASTIC MODULI USED IN THE INVERSION EXPERIMENTS

The matrix of the density-normalized elastic moduli $(\mathrm{km\,s^{-1}})^2$ of the orthorhombic medium (Schoenberg & Helbig 1997) reads

$$\begin{pmatrix} 9. & 3.6 & 2.25 & 0 & 0 & 0 \\ & 9.84 & 2.4 & 0 & 0 & 0 \\ & & 5.9375 & 0 & 0 & 0 \\ & & & 2. & 0 & 0 \\ & & & & 1.6 & 0 \\ & & & & & 2.182 \end{pmatrix}. \tag{C1}$$

Values of corresponding anisotropy parameters can be found in Table 1.